# Transition-State Theory Based Modeling of the Dynamics of the $O^+(^4S) + CO_2$ Reaction

**Ellen F. Sawilowsky and Stephen J. Klippenstein**

*Chemistry Department, Case Western Reserve University, Cleveland, Ohio 44106-7078*

*Received: April 27, 1998; In Final Form: August 21, 1998*

Transition-state theory based procedures for modeling the collision energy and internal temperature dependence of ion−molecule reactions are illustrated through a sample study of the $O^+(^4S) + CO_2$ reaction. Specific attention is paid to the effect of both short- and long-range interactions in the potential. Quantum chemical evaluations at the MP2/6-311G*+ level provide the data for a representation of the $O^+\cdots CO_2$ bending potential at arbitrary separations. A variable reaction coordinate transition-state theory formalism is employed in an unsuccessful search for a short-range transition state with a reactive flux below that predicted by phase-space theory. However, the short-range bonding interactions are still important in providing an effective lower bound for the location of the transition state. A satisfactory description of the experimental data for this reaction is obtained via the incorporation of a constant intersystem crossing (or perhaps energy randomization) rate constant of about $1 \times 10^{11}$ $s^{-1}$ for the transition from a quartet to a doublet $CO_3^+$ complex. This intersystem crossing is a prerequisite to the production of the low-energy product $^2O_2^+ + CO$.

## I. Introduction

An interesting question for barrierless reactions, in general, regards the extent to which short-range atom−atom repulsions reduce the reactive flux below that predicted on the basis of just the long-range potential. For radical−radical reactions, such steric effects clearly play an important role in determining the transition-state location and partition function.[1] For ion−molecule reactions, the increased strength of the long-range interactions leads to transition states which lie at much greater intermolecular separations. As a result, the importance of these short-range repulsions is less clear. For the specfic case of the H atom loss from benzene cation, these short-range repulsions lead to a substantial reduction in the rate constant below that predicted by phase-space theory (PST),[2] where only the long-range potential is considered.[3] In contrast, for the reaction of $Cl^-$ with $CH_3Cl$, the high-pressure association rate constant is solely determined by the long-range ion−dipole plus ion-induced dipole interactions.[4] For a number of other ionic reactions involving larger organic species, the presence of a secondary transition state due to these short-range repulsions has been postulated to explain various experimental data (see, e.g., refs 5−7).

In this work, we consider the possible importance of short-range interactions for the reaction of $O^+(^4S)$ with $CO_2$. The long-range attraction for this reaction lies between those for the aforementioned reactions since there is no dipole moment in $CO_2$, but its polarizability and quadrupole moment are much greater than that of the H atom. Correspondingly, one might expect this reaction to provide an interesting intermediate situation where the short-range interactions are of importance, but perhaps only for quite high energies where the transition state has moved to short separations. The experimental finding that the rate constant for this reaction decreases with increasing kinetic energy lends credence to this idea.[8−11] In particular, one possible explanation for the experimental observation is that the transition state moves in to shorter $O^+\cdots CO_2$ separations with increasing kinetic energy. Then, as this separation gets smaller, the short-range repulsions between the two fragments increase in importance, leading to a gradual reduction in the rate consant.

In analyzing this question, we employ our variable reaction coordinate implementation of transition-state theory (VRC-TST).[12] This approach requires a quantitative estimate for the $O^+\cdots CO_2$ interaction energies for the range of separations important to the determination of the transition state. These interaction energies are obtained here from a spline fit to a series of ab initio quantum chemical evaluations at the MP2/6-311G*+ level as outlined in section II.

The present VRC-TST calculations do not provide an explanation for the observed decrease in the rate constant with increasing collision energy. Thus, for completeness a model based on an alternative explanation is also explored here. In particular, the full reaction scheme involves three separate product channels:

$$O^+(^4S) + CO_2 \rightarrow CO_3^{+*} \rightarrow CO_3^+ \qquad \Delta H^\circ_{rxn} = -1.06 \text{ eV} \quad (1a)$$

$$\rightarrow {}^2O_2{}^+ + CO \qquad \Delta H^\circ_{rxn} = -1.19 \text{ eV} \quad (1b)$$

$$\rightarrow CO_2{}^+ + O \qquad \Delta H^\circ_{rxn} = 0.155 \text{ eV} \quad (1c)$$

The experiments of refs 8−11 were performed under low-pressure conditions where channel 1a is of negligible importance. One may then expect channel 1b to be the dominant product channel (at least for not too high a collision energy). Notably, this channel requires an intersystem crossing from the quartet state of the energized $CO_3^+$ complex prior to the production of the doublet $O_2^+ + CO$ products. At high enough energies, the redissociation of the $CO_3^+$ complex back to reactants may become faster than this intersystem crossing. As a result, the rate for loss of reactants would be reduced by the fraction of molecules which return to reactants instead of proceeding on to products. An analogous explanation, and perhaps equally likely, is that an increasing fraction of the energized complexes recross the transition state and return to reactants prior to the randomization of energy within the energized complex.

10.1021/jp9820020 CCC: $15.00 
Published on Web 11/03/1998

A second component of this work then involves an analysis of the full reaction scheme where the combined effect of the slow intersystem crossing and/or energy randomization rates are treated as a free parameter in the fitting of the experimentally observed rate constants. The procedures employed in this transition-state theory based modeling of the experimentally observed rate constants are summarized in section III.

The results from both the VRC-TST calculations for the association kinetics and the complete kinetic modeling are presented in section IV. One of the useful results from the VRC-TST calculations is a more quantitative prediction for the location of the transition state (TS). This location plays an important role in the consideration of possible short-range cutoffs in the TS location.[13,14] Such cutoffs have been suggested to provide an explanation for the experimental observations for related reactions of an *increase* in the reaction rate with increasing kinetic energy.[14,15] Some discussion of such effects is also provided in section IV. Finally, some concluding remarks are made in section V.

## II. Interaction Energies

A wide-ranging representation of the potential-energy surface is required in order to implement transition-state theory based investigations of the effect of both the short-range and anisotropic long-range interactions on the reaction dynamics. Here, estimates for these interactions were obtained on the basis of a series of quantum chemical evaluations employing second-order Møller Plesset perturbation theory (MP2).[16−19] These evaluations employed the 6-311G*+ basis set which is of double-$\zeta$ valence quality and includes single sets of both polarization functions and diffuse functions.[17,20] The Gaussian 92 and Gaussian 86 quantum chemical software were employed in the quantum chemical simulations described here.[21,22] No indication of important spin contamination was noted for either the quartet or the doublet states considered here (i.e., $\langle S^2 \rangle$ was generally within 0.02 of 3.75 for the quartet states and within 0.02 of 0.75 for the doublet states).

In a barrierless reaction, the two reacting fragments are typically only weakly interacting in the neighborhood of the transition state. As a result, it is generally acceptable to hold the structures of the ion and the molecule fixed at their infinite separation values during the determination of the interaction energies. Here, the $CO_2$ fragment was constrained to be linear and the CO bond lengths were held at 1.1787 Å.[23] The interaction energies then depend on only the two coordinates $R$ and $\theta$ defining the distance and orientation of the $O^+$ ion relative to the center-of-mass of the $CO_2$ fragment. By symmetry, the angle $\theta$, which is defined here as the angle between the $CO_2$ internuclear axis and the line-of-centers, only needs to be considered in the range from 0° to 90°.

The effect of relaxing the structures was examined for the equilibrium $^4CO_3^+$ structure. For a linear $^4CO_3^+$ structure, the MP2/6-311G*+ binding energy obtained for optimized CO bond lengths was 5635 $cm^{-1}$ while that obtained with the CO bond lengths fixed at 1.1787 Å was 5395 $cm^{-1}$. The optimized CO bond lengths for this linear structure were 1.1525 and 1.1876 Å, while the OO bond length was 2.1057 or 2.0896 Å for the fully and partially optimized structures, respectively. Thus, for a linear structure, there appears to be little effect of optimizing the CO bond lengths. At large separations, the linear structure is the lowest energy. However, at shorter separations, the covalent interactions lead to a planar minimum energy structure which is of $C_s$ symmetry. For the latter structure, a slightly greater, but still quite small, relaxation energy of 434 $cm^{-1}$ is obtained. In particular, constraining the $CO_2$ component to still be linear with bond lengths of 1.1787 Å yields a binding energy of 5554 $cm^{-1}$ for a C···O bond length $R$ of 3.0183 Å, and an OC···O bending angle $\theta$ of 27.4°. Meanwhile, the fully optimized $C_s$ symmetry structure has a binding energy of 5988 $cm^{-1}$, corresponding to CO bond lengths of 1.1491 and 1.2022 Å, an OCO bending angle of 149.7°, a C···O bond length $R$ of 2.9143 Å, and an OC···O bending angle $\theta$ of 32.4°.

**TABLE 1: Electrostatic Parameters for $CO_2$**

| parameter | ab initio | fit | expt |
|---|---|---|---|
| $Q$ (D − Å) | −4.55 | −4.75 | −4.4[a] |
| $\alpha_\perp$ (Å$^3$) | 1.33 | 1.68 | 1.97[b] |
| $\alpha_\parallel$ (Å$^3$) | 4.17 | 3.68 | 4.01[b] |
| $\langle\alpha\rangle$ (Å$^3$) | 2.28 | 2.35 | 2.65[b] |

[a] From ref 24. [b] From ref 25.

The restriction to two coordinates, $R$ and $\theta$, greatly simplifies the development of a potential. In particular, for intermediate and shorter separations, ab initio evaluations on a grid of points allows for the determination of the potential at arbitrary $R$ and $\theta$ via a cubic spline fit. Meanwhile, at larger separations, the potential is closely approximated by its long-range form which consists of a sum of ion-quadrupole and anisotropic ion-induced dipole interactions:

$$V = -\frac{q^2}{2R^4}(\alpha_\parallel \cos^2\theta_q + \alpha_\perp \sin^2\theta_q) + \frac{qQ(3\cos^2\theta_q - 1)}{2R^3} \quad (2)$$

Two separate grids were used for the intermediate separations. The first consisted of $R$ values ranging from 3.7 to 6.9 Å with a 0.4 Å spacing. A more finely spaced grid of 0.2 Å spacing was employed for separations ranging from 1.9 to 3.7 Å, where the potential is more rapidly varying. At 1.9 Å separation, the potential is strongly repulsive for all orientations and, thus, no calculations were required for shorter $R$s. Angular grids of 15° spacing were used for both regions.

Sample evaluations of the basis-set superposition errors (BSSE) indicated that they were of negligible importance (e.g., for linear geometries the BSSE was found to be 0.5, 27, and 148 $cm^{-1}$ for $R$ values of 8.0, 6.0, and 4.0 Å, respectively), and so no corrections for the BSSE were included here.

The long-range portion of the potential has been generated here via a fit of the quadrupole moment and the parallel and perpindicular polarizabilities to a set of ab initio data for $R$ ranging from 8.0 to 12.0 Å at angles of 0°, 30°, 60°, and 90°. Alternatively, one could simply employ the ab initio or experimental values for these parameters. The two sets of parameters are tabulated in Table 1 together with the corresponding experimental values. The minor difference between the fitted and calculated ab initio parameters may be indicative of either BSSE in the supermolecule calculations or alternatively of minor deviations from the purely long-range form. Importantly, each of the two ab initio sets are in good agreement with the experimental data, and so it matters little which particular parameter set is employed.

The accuracy of the fit at long range is illustrated in Figure 1, where the $R$ dependence of the fitted and ab initio data are plotted for various angles. However, at separations of about 7 Å, the ab initio data begins to diverge from the long-range analytical form of eq 2, becoming increasingly more attractive than the analytical data with decreasing separation. Thus, for separations of 6.9 Å and below, the analytical form is replaced with a spline fit to the grid of ab initio data. Here, we have chosen to employ the fitted ab initio parameters for the long-

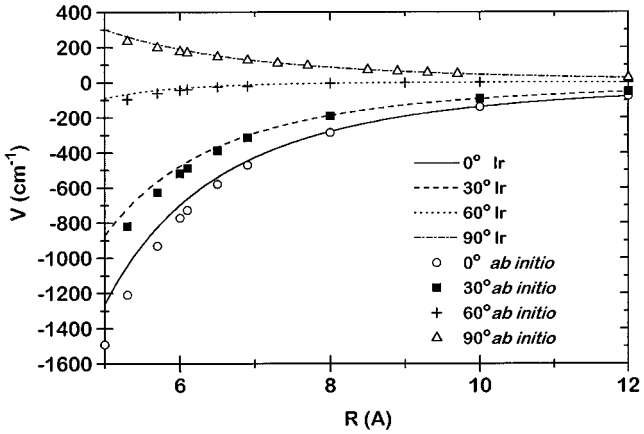


**Figure 1.** Plot of the fitted analytical potential and the ab initio data as a function of the separation distance for $\theta = 0°$ (solid lines, open circles), $\theta = 30°$ (dashed line, solid squares), $\theta = 60°$ (dotted line, pluses), and $\theta = 90°$ (dashed−dotted line, open triangles).

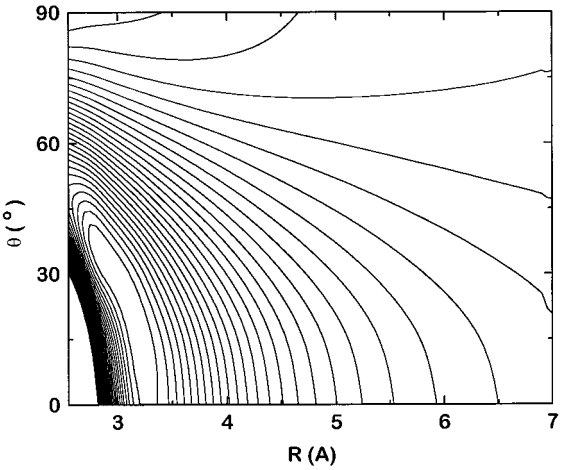


**Figure 2.** Contour plot of the interaction between $CO_2$ and $O^+$. The spacing between contours is 226 $cm^{-1}$. The highest contour, at the top left, is at 548 $cm^{-1}$, while the lowest contour is at −5328 $cm^{-1}$.

range analytical form in order to obtain a smooth transition to the short-range grid-based spline fits.

A contour plot of the potential for separations ranging from 2.5 to 7.0 Å is provided in Figure 2. This plot illustrates the wide range of orientations for which the $O^+\cdots CO_2$ interactions are attractive. Only the three highest contours (and their analogues at a small separation distance and angle) are repulsive; this repulsivity is generally much weaker than the attractiveness. At large separations, the reaction path is along the linear geometry ($\theta = 0°$), where both the quadrupole and induced dipole interactions are attractive. At a separation of about 3.3 Å, the bending angle begins to increase along the reaction path until the optimum value of about 32° is reached at a separation of about 2.9 Å. The minor discontinuities at $R = 6.9$ Å are indicative of the minor deviations between the fitted long-range potential and the ab initio data.

The kinetic estimates described below also require thermodynamic parameters for the equilibrium $CO_3^+$ structure. The vibrational frequencies for this structure are obtained here from ab initio evaluations at the MP2/6-31G* level and are reported in Table 2. Meanwhile, the binding energy of $CO_3^+$ is evaluated on the basis of G2(MP2) theory,[27] which is a recently described variant of the original Gaussian-2 (G2) theory.[28] The G2(MP2) theoretical method provides a well-defined procedure for estimating the equilibrium energetics of molecules with an

**TABLE 2: Vibrational Frequencies**

| species | $\nu_1$ | $\nu_2$ | $\nu_3$ | $\nu_4$ | $\nu_5$ | $\nu_6$ |
|---|---|---|---|---|---|---|
| $CO_3^+$ | 123[a] | 454 | 581 | 626 | 1264 | 2352 |
| $CO_2$ | 655(667)[b] | 655(667) | 1335(1388) | 2433(2349) | | |
| $CO_2^+$ | 561 | 602 | 1040 | 2782 | | |

[a] Frequencies in $cm^{-1}$ from MP2/6-31G* calculations. [b] Numbers in parentheses denote experimental frequencies from ref 26.

estimated accuracy of about 1000 $cm^{-1}$ or better.[28] This method is based on an initial determination of the structure and frequencies of the relevant stationary point at the MP2/6-31G* level. A reference energy is then evaluated at the QCISD(T)/6-311G* level for these MP2/6-31G* optimized structures.[29] Corrections for more extended basis sets and zero-point energy effects are then appended to this reference energy. An ad hoc higher level correction is also included to incorporate in an average fashion any remaining deficiencies which depend on the number of chemical bonds. Two minor modifications to the original G2(MP2) method are made here. First, the core electrons are frozen in the MP2/6-31G* optimizations, which should yield negligible further errors in the geometrical structures. Furthermore, since the vibrational frequencies play such an important role in the transition-state theory evaluations, they were obtained here at the MP2/6-31G* level instead of the HF/6-31G* level. The zero-point corrected binding energy $D_0$ of the complex is then estimated to be 8553 $cm^{-1}$.

The analysis of the charge-transfer kinetics also requires thermodynamic parameters for $CO_2^+$ and the O atom. The vibrational frequencies for this species were again obtained at the MP2/6-31G* level and are also reported in Table 2, as are the corresponding neutral frequencies. For the latter quantity the experimental values are also available and were employed in the actual calculations.[26] At the MP2/6-31G* level $CO_2^+$ is linear but with two different CO bond lengths of 1.1149 and 1.2752 Å. For the O atom a polarizability of 0.80 $Å^3$ was used.[30]

### III. Transition-State Theory Based Kinetic Modeling

The various experiments[8−11] observed the rate of reaction for thermal $CO_2$ colliding with $O^+$ ions (primarily in the ground $^4S$ state) with collision energies centered about a specific value. In ref 8, both the temperature and the collision energy were varied, while in refs 9−11, only the collision energy was varied. For the conditions of thermal $CO_2$ colliding with $O^+$ at a given collision energy $E_t$, the reaction rate constant for producing a particular product channel $i$ may be written as[31,32]

$$k_i(E_t, T) = \frac{1}{hQ_{\rm rot}(T)Q_{\rm vib}(T)\rho_t(E_t)} \sum_{J,l,j,\mathbf{v}} N_0(E_t, J, l, j, \mathbf{v}) \times \exp[-\beta (E_j + E_{\mathbf{v}})] P_i(E, J) \quad (3)$$

where $j$ and $\mathbf{v}$ are the rotational and vibrational quantum numbers for $CO_2$, respectively, and $E = E_t + E_j + E_v$. The quantities $Q_{\rm rot}$ and $Q_{\rm vib}$ are the corresponding rotational and vibrational partition functions for $CO_2$, respectively. The translational density of states, $\rho_t(E_t)$, is given by $[\mu^3 E_t/2\pi^4\hbar^6]^{1/2}$ with $\mu$ being the reduced mass for the $O^+$, $CO_2$ collision. The quantity $P_i$ in eq 3 is the probability for decomposition of the initially formed complex into the product channel $i$.

The total reaction probability, $N_0$, in eq 3 is that for formation of the initial $^4CO_3^+$ ion−molecule complex from a collision between reactants at energy $E_t$, total angular momentum $J$, orbital angular momentum $l$, and in the internal rovibrational

states specified by $j$ and $\mathbf{v}$. Within PST (i.e., the Langevin model), this reaction probability is represented by the number of available states with the particular quantum numbers $j$, $l$, $\mathbf{v}$:

$$N_0^{\mathrm{PST}}(E_t, J, j, l, \mathbf{v}) = \Theta(E_t - E_l^{\dagger})\Delta(l, j, J)(2J+1) \quad (4)$$

where the step function and triangle inequalities ensure conservation of energy and total angular momentum, respectively. The absence of any vibrational state dependence to this number of states arises from the assumption of vibrational adiabaticity and the neglect of any variation in the vibrational energies from separated fragments through the transition state. The implementation of PST then requires solely the determination of the effective centrifugal barriers $E_l^{\dagger}$ for some model spherically symmetric long-range potential.

Within PST, one assumes that both the orbital and fragment rotational angular momentum are conserved from reactants on through to the complex formation transition state. In contrast, within transition-state theory (TST), one instead assumes that these quantities are strongly mixed, producing statistical distributions. In this instance, one should replace $N_0$ of eq 4 with

$$N_0^{\mathrm{TST}} = N_0^{\mathrm{PST}}(E_t, J, j, l, \mathbf{v}) \frac{N_0^{\dagger}(E_t + E_j, J, \mathbf{v})}{N_0^{\mathrm{PST}}(E_t + E_j, J, \mathbf{v})} \quad (5)$$

where $N_0^{\dagger}$, is the number of available states at the transition state (for given vibrational state $\mathbf{v}$) assuming complete mixing of the rotational and translational states of the fragments. This quantity depends only on the total energy in these rotational and translational modes and on $J$. In writing this expression, we have retained the adiabaticity assumption for the vibrational modes of $CO_2$. With this assumption, only the contribution from the interfragment modes, commonly termed the transitional modes, is included in the evaluation of $N_0^{\dagger}$. The variable reaction coordinate VRC-TST formalism is employed in the evaluation of $N_0^{\dagger}$ for these transitional modes as summarized in section IVA below. The total PST number of states for given vibrational state $\mathbf{v}$ in eq 5 is given by

$$N_0^{\mathrm{PST}}(E, J, \mathbf{v}) = \sum_{l,j} \Delta(l, j, J)(2j + 1)\Theta(E - E_l^{\dagger} - E_j) \quad (6)$$

with $E = E_t + E_j$.

For the probability $P_i$ we make the standard statistical assumption of a total randomization of the energy within this weakly bound complex prior to its redissociation. At the highest energies considered below, this assumption may be of limited validity due to the shortness of the lifetime for the weakly bound ion−molecule complex that is initially formed. However, the extent of the agreement between the observations and the predictions within this statistical framework should still be informative. In general, this assumption may be expected to be most appropriate at the lowest collision energies where the complex lifetimes are relatively large.

The specific transition-state theory expression for $P_i$ is given by

$$P_i(E, J) = \frac{N_i^{\dagger}(E, J)}{\sum_i N_i^{\dagger}(E, J)} \quad (7)$$

where $N_i^{\dagger}(E,J)$ is the total number of available states at the transition state leading to channel $i$. The present applications require the consideration of three separate channels: the reactants [labeled channel 0] and the products arising from channels 1b and 1c. For channel 0, $N_0^{\dagger}$ is determined within the VRC-TST formalism employing the ab initio potential described in section II.

The production of $O_2^+ + CO$ must be preceded by an intersystem crossing from the reactant quartet state to a doublet state. This intersystem crossing likely provides the bottleneck for the dissociation of the $CO_3^+$ complex into the channel 1b products. Unfortunately, it is difficult to obtain an a priori estimate for the rate of this intersystem-crossing process. The overall reaction rate is strongly dependent on this rate constant $k_{\mathrm{ISC}}$, and so we, instead, treat it as a single fitting parameter in the final comparisons with experiment. For simplicity, this rate is considered to be independent of energy and total angular momentum. In essence, the resulting fitted value is really an average over its true values for the regions most strongly dependent on the particular value. With this assumption, the quantity $N_{1b}^{\dagger}$ is obtained from the relation

$$N_{1b}^{\dagger}(E, J) = k_{\mathrm{ISC}} h \rho_{CO_3^+}(E, J) \quad (8)$$

The number of states for the charge-transfer channel (1c) is obtained from standard PST calculations employing the ion-induced dipole potential. TST-type evaluations analogous to those described below for channel 0 could also have been implemented for this channel. However, the endothermicity for this channel suggests that it is of only secondary importance, and thus, the more easily implemented PST values should be satisfactory for at least a qualitative indication of its effect.

Finally, the reaction probabilities $P_i$ are assumed to be independent of $J$ and are simply evaluated for $J = 0$. Such a simplification seems appropriate in light of the absence of any a priori information on the intersystem-crossing rate constant.

## IV. Results and Discussion

**A. Complex Formation.** The transition-state number of states for the "transitional" modes is evaluated here with a variable reaction coordinate (VRC) phase-space integral-based methodology.[12,33] The essence of this approach involves the definition of the dividing surface in terms of a fixed distance $r$ between the $O^+$ ion and a point $x$ along the $CO_2$ axis (cf. Figure 3). The point $x$ is located a distance $R_{11}$ away from one of the O atoms in $CO_2$. A $R_{11}$ value of 1.1780 Å corresponds to a standard center-of-mass separation distance (CMSD) reaction coordinate, while a value of 0 corresponds to a bond length reaction coordinate. The minimum value of the number of available states $N_0(E,J,r,R_{11})$ evaluated on a grid of $r$ and $R_{11}$ values then provides the VRC-TST estimate to the transition-state number of states $N_0^{\dagger}$. The Monte Carlo phase-space integral-based algorithm described in ref 12 was employed in the present evaluations of $N_0(E,J,r,R_{11})$. The Monte Carlo integrations were typically performed with enough sampling points to obtain on the order of 1−2% uncertainties.

Sample evaluations generally found two minima in $N_0$. One minima corresponds to the typical PST-like transition state with a $R_{11}^{\dagger}$ value near 1.1780 Å (i.e., a CMSD reaction coordinate) and quite large values of $r^{\dagger}$ (e.g., 6 Å). The second minimum typically corresponded to slightly negative values (e.g., −0.4 Å) for $R_{11}^{\dagger}$ and substantially smaller values for $r^{\dagger}$. The latter $N_0^{\dagger}$ values were often lower than those obtained for the CMSD reaction coordinate (particularly at higher energies) but never by more than a factor of 2.0. Ordinarily one would interpret these values as corresponding to an inner transition state which sometimes provides a greater bottleneck for the reactive flux than does the outer PST-like transition state. However, further

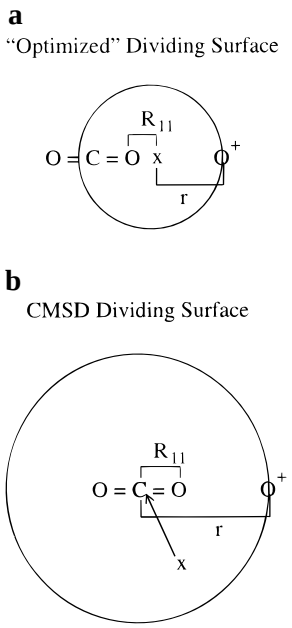


**Figure 3.** Schematic diagram of sample transition-state dividing surfaces for (a) the optimized and (b) the CMSD reaction coordinates. The solid circles denote the range of motion for $O^+$ relative to $CO_2$ on the dividing surface.

consideration of the symmetry of $CO_2$ suggests that this interpretation is actually incorrect for $CO_2$. In particular, one requirement for the transition-state dividing surface is that it separates the reactants from the products. The symmetry of $CO_2$ results in the presence of two equivalent $CO_3^+$ minima: one on either side of the central C at $\theta$ values of 32° and 148°. The optimized inner transition-state dividing surface separates one of these minima from the reactants (cf., the schematic illustration of the optimized dividing surface provided in Figure 3a). However, the other minima is on the reactant side of the dividing surface (cf., the left-hand side of Figure 3a, which is all outside the dividing surface). In contrast, the CMSD dividing surface properly separates the two minima from the reactants (i.e., both minima are inside the circle in Figure 3b). In essence, one would need to consider two separate dividing surfaces and sum the reactive flux from each in order to obtain the total reactive flux when employing the optimized inner dividing surface. With this doubling of the number of states, the inner transition state $N_0^\dagger$ is then always greater than that for the CMSD $N_0^\dagger$. Thus, we conclude that we find no evidence here for a reaction coordinate that deviates from the CMSD for this reaction.

The following results are all based on the CMSD reaction coordinate, labeled *R* here. The variation in the transition-state location $R^\dagger$ as a function of *E* is plotted in Figure 4 for various *J* values. For any given *J*, as the energy increases, the transition state gradually moves in to shorter and shorter separation. At very high energies (i.e., above about 8000−12000 $cm^{-1}$ for the high *J* values), the transition state actually disappears as the number of states simply monotonically decreases with decreasing *R*. However, in these instances, the range of *R* from about 4 to 5 Å corresponds effectively to a plateau in *N* with little variation with *R*. Thus, in these instances we have simply taken $N^\dagger$ to be the value of *N* at $R = 3.8$ Å.

It is interesting to consider the differences between the present phase-space integral-based estimates for $N_0^\dagger$, obtained for the full potential, and the corresponding PST result which considers only the ion-induced dipole potential. The ratio of these two numbers is plotted versus energy in Figure 5, again for a range

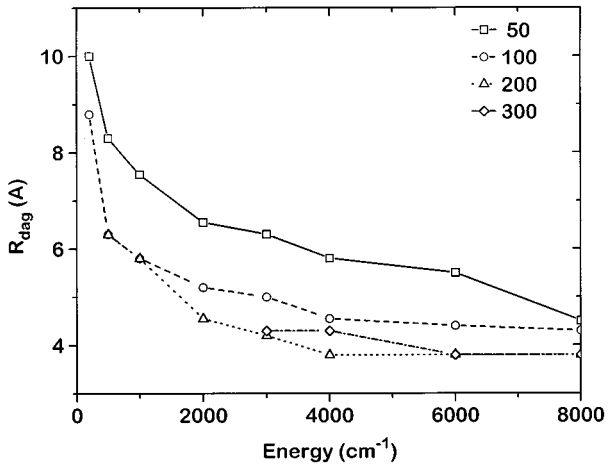


**Figure 4.** Plot of the transition state location $R^\dagger$ versus energy for *J* values of 50 (squares and solid line), 100 (circles and dashed line), 200 (triangles and dotted line), and 300 (diamonds and dashed−dotted line).

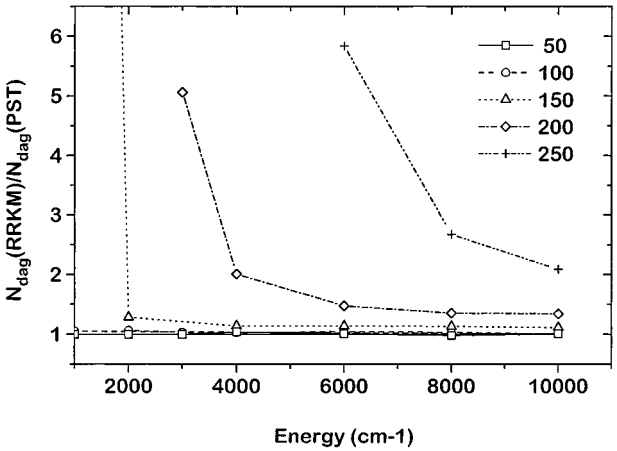


**Figure 5.** Plot of the ratio of the VRC-TST-calculated *N* to the PST-calculated *N* as a function of energy for *J* values of 50 (squares and solid line), 100 (circles and dashed line), 150 (triangles and dotted line), 200 (diamonds and dashed−dotted line), and 250 (pluses and dashed−dot-dot line).

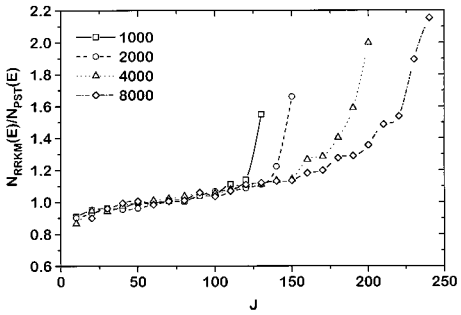


**Figure 6.** As in Figure 5, but as a function of *J* for *E* values of 1000 (squares and solid line), 2000 (circles and dashed line), 4000 (triangles and dotted line), and 8000 $cm^{-1}$ (diamonds and dashed−dotted line).

of *J* values, and versus *J* for a range of *E* in Figure 6. For each *J* in Figure 5, the ratio is seen to decrease with increasing energy due to the decreasing importance of the ion-quadrupolar interactions. Similar observations (both in form and in magnitude) have been noted in a number of previous experimental and theoretical studies, with the latter studies focusing on purely thermal conditions.[34,35] At higher *J*s, the ratio deviates from unity to a much greater extent. This increase in the deviation is likely an indication of the importance of the covalent

interactions in increasing the attractiveness of the potential beyond that predicted by the long-range form. A similar observation has been noted by Clary and co-workers for the $C^+ + HCl$ reaction.[36]

Another factor which contributes to the deviation of this ratio from unity is the fact that PST incorporates an assumed conservation of the orbital angular momentum $l$ and thereby separate transition states for each $l$. It is perhaps worth noting that this conservation of $l$ in PST implies that PST is no longer a proper statistical variational theory, since $l$ is not absolutely conserved. The present variational transition-state theory maintains the variational character (within a statistical framework) by instead employing a single transition state for all of the $l$-dependent states for a given $J$. As a result, the variational results will exceed the PST results, and this will be most dramatic when the orbital barriers are an important factor.[37] Correspondingly, one might expect relatively large deviations from unity for the ratio at low $E$ for a given $J$ or equivalently for high $J$ at a given $E$, just as observed in Figures 5 and 6. However, it is worth noting that in separate calculations of the thermal rate constants for various ion−molecule reactions,[38] the variational results reproduce analytical PST results to within 1−2%, suggesting that this deviation is generally very minor. Thus, we ascribe the substantial differences observed in Figures 5 and 6 to differences in the potential.

The increase in the ratio at high energies (cf. Figure 6) may be directly related to the increase in the rate constant observed by Lindinger and co-workers in their experimental studies, which they have attributed to the effect of hard-sphere interactions.[14,15] To examine this relation more closely, we have first evaluated the high-pressure rate constant for the present $O^+ + CO_2$ reaction as a function of collision energy (i.e., under the assumption of zero probability for redissociation back to reactants). The ratio of the predicted rate constant for the full potential to the Langevin rate constant then corresponds to an observable quantity which Lindinger and co-workers have generally labeled as $\beta$.

Unfortunately, calculations for the highest energies (where this upturn is expected to arise) are complicated by the fact that a plot of the variationally determined number of states versus separation monotonically decreases to zero as the separation is decreased. As a result, the proper transition-state number of states is uncertain. Of course, the dividing surface cannot be located at too short a separation distance or it does not separate reactants and products. Instead, reactants and products would both be on one side of the dividing surface. With no clear minimum in the plot, one is forced to assume some minimum separation for the consideration of the transition state. If this minimum separation is large enough to properly separate reactants and products, then one maintains the variational character of the theory. Conversely, if it is too small, then the dividing surfaces are not proper dividing surfaces and the numbers obtained are meaningless.

For the present reaction, we find that the plots of the number of states versus separation maintain a near-plateau region down to separations of about 3.8 Å. For smaller separations, they begin to decrease much more rapidly. Furthermore, consideration of the potential-energy surface contour plot in Figure 2 suggests that this value corresponds to a physically reasonable separation of reactants and products.

Within PST, the assumption of a purely attractive ion-induced dipole potential implies that effective barriers and corresponding transition states are always present. However, at high enough energies, the transition-state separations become so small as to be clearly incorrect. The implementation of a minimum effective barrier location within PST then provides an ad hoc correction which leads to a result that is always greater than the uncorrected (Langevin) result.

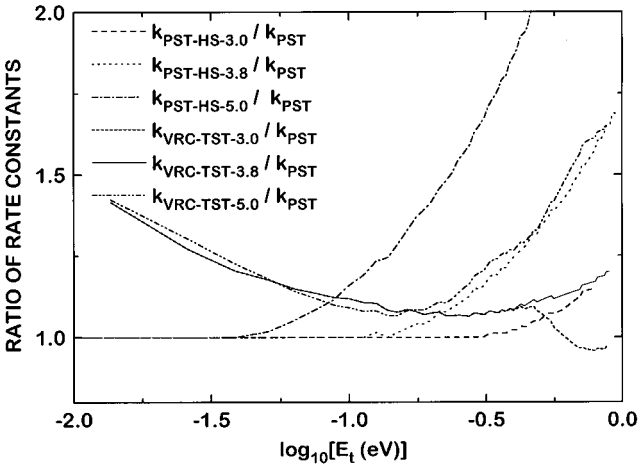


**Figure 7.** Plot of the cutoff-corrected PST- and VRC-TST-calculated association rate constant relative to the full PST rate constant as a function of the collision energy $E_t$ for a temperature of 303 K. Cutoffs of 3.0, 3.8 and 5.0 Å are considered.

A plot of this $\beta$ versus collision energy is provided in Figure 7 for a reactant temperature of 303 K. Included in this plot are results obtained according to both VRC-TST and PST, assuming minimum separations for the transition state of 5.0, 3.8, and 3.0 Å.

The ratio of the modified PST result to the Langevin result increases with increasing energy and does so more rapidly for larger cutoffs. The magnitude of this rise is solely indicative of the magnitude of the available phase space at the given cutoff relative to that at the $l$-dependent effective barrier for the long-range ion-induced dipole potential. Comparison with Figure 2 of ref 14 suggests that a seemingly reasonable cutoff of about 3.5 Å within PST would roughly reproduce the observed $\beta$ dependence for a variety of reactions.

For the VRC-TST calculations, the effect of the cutoffs is considerably weaker. The best estimate of 3.8 Å for the actual region at which the complex has been reached gives a curve which is closely analogous to that observed for related reactions in the experimental studies of Lindinger and co-workers.[14,15] A cutoff of about 4.0 Å would likely correspond to an optimum value for such comparisons. For this optimum cutoff, the increase at high energies is initially due to the increasing attractiveness of the potential as compared to the long-range potential. Ultimately, however, the cutoff also begins to play a role, as seen by the deviations between the data for the cutoffs of 3.8 and 3.0 Å. The rise with decreasing energies at low energies is indicative of the increasing importance of the ion-quadrupole potential.

The cutoff of 5.0 is unrealistically large and correspondingly causes an unrealistically large increase in the rate constant with collision energy at high collision energies. In contrast, the cutoff of 3.0 Å is unrealistically low and corresponds to a further drop in the transition-state estimates as the repulsive wall of the potential begins to be sampled (cf. Figure 2). In summary, the value of 3.8 Å corresponds closely to the end of the plateau region in the plot of the number of states versus separation and, thus, provides the best a priori estimate for the true cutoff. The good agreement with the observed rate versus collision energy dependence for related reactions for this cutoff suggests that a

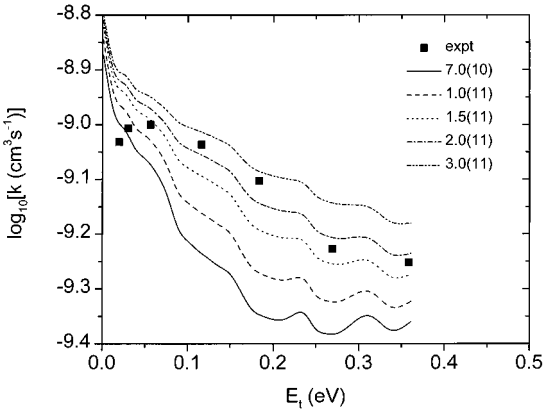


**Figure 8.** Plot of the experimental data from ref 8 (solid squares) and the present theoretical results (lines) for the loss of $O^+$ as a function of center-of-mass collision energy $E_t$ at a temperature of 151 K. The solid, dashed, dotted, dashed−dotted, and dashed−dot-dot lines are for assumed intersystem crossing rates of 0.7, 1, 1.5, 2, and $3 \times 10^{11}$ $s^{-1}$, respectively.

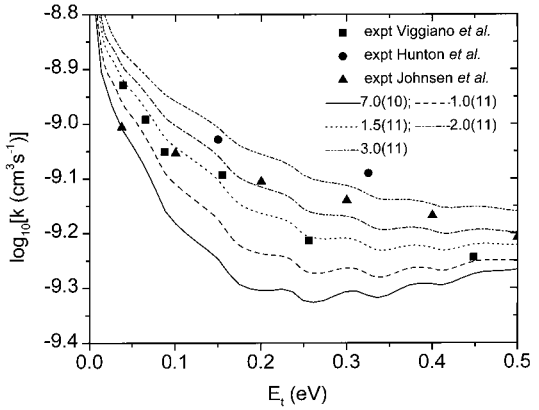


**Figure 9.** As in Figure 8 but for the reactants at a temperature of 303 K. Also, the experimental data from refs 9 and 10 are plotted as the solid triangles and solid circles, respectively.

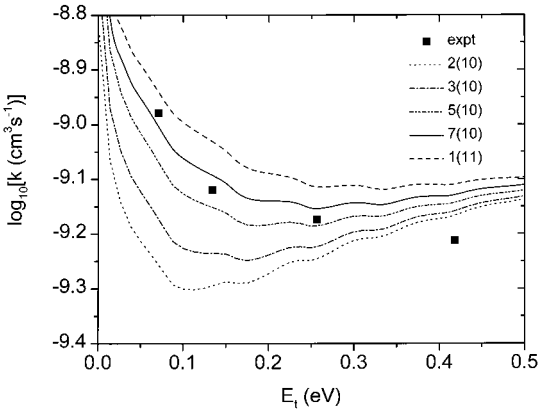


**Figure 10.** As in Figure 9 but for a temperature of 545 K, and with the lines for 1.5, 2, and $3 \times 10^{11}$ $s^{-1}$ replaced with lines for 2, 3, and $5 \times 10^{10}$ $s^{-1}$.

satisfactory description of the association dynamics is being obtained.

**B. Reaction Rate Constant.** The above discussion suggests that the present variational TST modeling provides a reasonable description of the various failures of the Langevin model for the complex formation rate constant. However, the failure to determine a reduction in the entrance channel transition-state number of states below the phase-space theory $(PST)^2$ value implies that the complex formation rate alone will not decrease below the Langevin value at high collision energies (cf., Figure 7). Thus, it is necessary to postulate an alternative bottleneck to the reaction which arises at higher energies. One especially good candidate for such a bottleneck is the intersystem crossing from the initially formed quartet $CO_3^+$ complex to a doublet species which produces the low-energy products. At low energies, this rate may be rapid enough to allow complete conversion to products. However, as the energy rises, the redissociation rate to reactants will rapidly increase and may become competitive with the intersystem-crossing rate. Alternatively, one might consider the rate of energy randomization within the complex to provide the secondary bottleneck to reaction.

Here, the intersystem-crossing (or energy randomization) rate was employed as a single fitting parameter in the modeling of the experimental data of refs 8−10. Sample plots of the predicted collision energy dependence for the rate constant are provided in Figures 8−10, for temperatures of 151, 303, and 545 K, respectively. Note that within the present theoretical model the drop in the rate constant below the Langevin rate is solely due to the addition of the intersystem-crossing bottleneck. Reasonable fits to the data are obtained for intersystem-crossing rates $k_{ISC}$ of about $0.7-2 \times 10^{11}$ $s^{-1}$ for these temperatures. Rates of this magnitude do not seem unreasonable for either intersystem crossing or energy randomization bottlenecks. The best fit value for $k_{ISC}$ does vary some from plot to plot. This variation may simply suggest that the intersystem-crossing rate depends on energy, and as a result the fitted value depends on the details of the modeling. Interestingly, variation of $k_{ISC}$ by a factor of 2 from the best-fit value provides noticeably worse agreement in each case.

The leveling off and/or rise in the predicted rate at high energy is related to the turning on of the charge-transfer channel which was only modeled at the PST level here and with a focus on $J = 0$. Thus, the modest deviations at higher energies are not unexpected. Furthermore, for these energies, the validity of the statistical assumptions themselves become very doubtful. The drop with increasing collision energy for the theoretical predictions at low energy is related to the increasing importance of the back dissociation to reactants. We are unable to provide an explanation for the absence of a decrease at low $E$ for the experimental data at 151 $K$.

Viggiano et al. noted in ref 8 that the overall rate constant was essentially independent of $CO_2$ temperature. The present theoretical modeling similarly shows only a weak dependence on the $CO_2$ temperature, with the best fit $k_{ISC}$ being about a factor of 2 lower at 545 K. Furthermore, we note that the $CO_2^+$ branching fraction predicted by the present calculations is in, at least, qualitative agreement with the experimental data from refs 8−11. In particular, it is found to rise with both energy and temperature. For a temperature of 303 K, it takes the values of 10%, 50%, and 90% at translational energies of 0.13, 0.25, and 0.55 eV, respectively. The rise with energy occurs somewhat more rapidly than suggested by the experimental data, which may simply be indicative of the need to include the $J$ dependence of the transition-state numbers of states when evaluating the reaction probabilities $P_i$. The focus of this work is on the qualitative nature of the translational energy dependence of the net reaction rate constant, and so we find such qualitative agreement for the branching fractions to be satisfactory.

With the present model, the lifetime of the collision complex is predicted to be only on the order of 10 ps. For such short lifetimes, a variety of nonstatistical effects may arise. Thus,

the modeled $k_{ISC}$ should only be taken as a qualitative guide to the possible effect of a bottleneck to the intersystem crossing. In fact, bottlenecks in various other energy-transfer processes may also provide an explanation for the observations.

## V. Concluding Remarks

A variety of interesting observations were made in the present theoretical modeling of the reaction of $O^+(^4S)$ with $CO_2$. First, there is no indication of an inner transition state region separate from the outer PST like transition state. This absence of an inner transition state even though the long range interactions are quite weak, is related to the symmetry of the problem which leads to a not very anisotropic potential. As a result, the CMSD is the optimum reaction coordinate throughout (or at least within the family of dividing surfaces considered in the present VRC-TST approach) and there is no reduction beyond that predicted by PST.

The increased strength of the attractive interactions beyond the long-range ion-induced dipole plus ion-quadrupole form (cf. Figure 1) provides a reasonable explanation for the increase in the high-pressure association rate constant above the PST rate at high collision energies. The fact that the transition state must lie beyond some minimum separation also appears to be related to this rise at high energies. The predicted rise in the association rate constant for calculations employing a physically motivated minimum transition-state separation of 3.8 Å is in both qualitative and quantitative agreement with the experimental observations of Lindinger et al. for related systems.[14,15]

The experimentally observed decrease in the overall rate constant with increasing collision energy is in sharp contrast with that predicted by the theoretical modeling of solely the association process. This suggests that additional complications such as bottleneck(s) in intersystem crossing and/or energy randomization play an important role in this process. An estimate of about $1 \times 10^{11}$ $s^{-1}$ is obtained for the rate of passing through this bottleneck via comparison with the experimental data.

**Acknowledgment.** Support of this research through NSF Grant No. CHE-9423725 is gratefully acknowledged.

## References and Notes

(1) Klippenstein, S. J. In *The Chemical Dynamics and Kinetics of Small Radicals*; Liu, K., Wagner, A. F., Ed.; World Scientific: Singapore, 1996.

(2) Pechukas, P.; Light, J. C. *J. Chem. Phys.* **1965**, *42*, 3281. Pechukas, P.; Rankin, R.; Light, J. C. *J. Chem. Phys.* **1966**, *44*, 794. Nikitin, E. E. *Teor. Eksp. Khim. Acad. Nauk Ukr. SSR* **1965**, *1*, 135, 248. Klots, C. E. *J. Phys. Chem.* **1971**, *75*, 1526.

(3) Klippenstein, S. J.; Faulk, J. D.; Dunbar, R. C. *J. Chem. Phys.* **1993**, *98*, 243.

(4) Klippenstein, S. J. Unpublished results.

(5) Chesnavich, W. J.; Bass, L.; Su, T.; Bowers, M. T. *J. Chem. Phys.* **1981**, *74*, 2228. Webb, D. A.; Chesnavich, W. J. *J. Phys. Chem.* **1983**, *87*, 3791. Chesnavich, W. J. *J. Chem. Phys.* **1984**, *84*, 2615.

(6) Chronister, E. L.; Morton, T. H. *J. Am. Chem. Soc.* **1990**, *112*, 133.

(7) Meot-Ner, M.; Smith, S. C. *J. Am. Chem. Soc.* **1991**, *113*, 862.

(8) Viggiano, A. A.; Morris, R. A.; Van Doren, J. M.; Paulson, J. F. *J. Chem. Phys.* **1992**, *96*, 270.

(9) Johnsen, R.; Brown, H. L.; Bionid, M. A. *J. Chem. Phys.* **1970**, *52*, 5080.

(10) Hunton, D. E.; Viggiano, A. A.; Morris, R. A.; Paulson, J. F.; Smith, D.; Adams, N. G. *J. Geophys. Res.* **1991**, *96*, 13881.

(11) Flesch, G. D.; Ng, C. Y. *J. Geophys. Res.* **1991**, *96*, 21403.

(12) Klippenstein, S. J. *Chem. Phys. Lett.* **1990**, *170*, 71; *J. Chem. Phys.* **1991**, *94*, 6469; *J. Chem. Phys.* **1992**, *96*, 367.

(13) Smith, S. C.; McEwan, M. J.; Giles, K.; Smith, D.; Adams, N. G. *Int. J. Mass Spectrom. Ion Processes* **1990**, *96*, 77.

(14) Glosík, J.; Freysinger, W.; Hansel, A.; Španěl, P.; Lindinger, W. *J. Chem. Phys.* **1993**, *98*, 6995.

(15) Glosík, J.; Smith, D.; Španěl, P.; Freysinger, W.; Lindinger, W. *Int. J. Mass Spectrom. Ion Proceses* **1993**, *129*, 131.

(16) Szabo, A.; Ostlund, N. S. *Modern Quantum Chemistry: Introduction to Advanced Electronic Structure Theory*; McGraw-Hill: New York, 1982.

(17) Hehre, W. J.; Radom, L.; Schleyer, P. V. R.; Pople, J. A. *Ab Initio Molecular Orbital Theory*; Wiley-Interscience: New York, **1986**.

(18) Møller, C.; Plesset, M. S. *Phys. Rev.* **1934**, *46*, 618.

(19) Pople, J. A.; Binkley, J. S.; Seeger, R. *Int. J. Quantum Chem. Symp.* **1976**, *10*, 1.

(20) Krishnan, R.; Frisch, M. J.; Pople, J. A. *J. Chem. Phys.* **1980**, *72*, 4244. Frisch, M. J.; Pople, J. A.; Binkley, J. S. *J. Chem. Phys.* **1984**, *80*, 3265.

(21) Frisch, M. J.; Trucks, G. W.; Head-Gordon, M.; Gill, P. M. W.; Wong, M. W.; Foresman, J. B.; Johnson, B. G.; Schlegel, H. B.; Robb, M. A.; Replogle, E. S.; Gomperts, R.; Andres, J. L.; Raghavachari, K.; Binkley, J. S.; Gonzalez, C.; Martin, R. L.; Fox, D. J.; Defrees, D. J.; Baker, J.; Stewart, J. J. P.; Pople, J. A. *GAUSSIAN 92*, Gaussian Inc.: Pittsburgh, PA, 1992.

(22) Frisch, M. J.; Binkley, J. S.; Schlegel, H. B.; Raghavachari, K.; Melius, C. F.; Martin, R. L.; Stewart, J. J. P.; Bobrowicz, F. W.; Rohlfing, C. M.; Kahn, L. R.; Defrees, D. J.; Seeger, R.; Whiteside, R. A.; Fox, D. J.; Fleuder, E. M.; Pople, J. A. *GAUSSIAN 86*; Carnegie-Mellon Quantum Chemistry Publishing Uunit: Pittsburgh, PA, 1984.

(23) The experimental and MP2/6-311G*+ optimized values for $R_{CO}$ are 1.1600 and 1.1700 Å, respectively. Ideally, one would employ either of these two values in the evaluation of the interaction energies. The value of 1.1787 Å, which was accidentally employed here, should also be satisfactory as it differs by less than 0.02 Å from these two values.

(24) Su, T.; Bowers, M. T. *Int. J. Mass Spectrom. Ion Processes* **1975**, *17*, 309.

(25) Landolt, H. H.; Bernstein, R. B. *Zhlenwerte and Funktionen*, 3 Teil; Springer: Berlin, 1950; p 509.

(26) Steinfeld, J. I. *Molecules and Radiation: An Introduction to Modern Molecular Spectroscopy*, 2nd ed.; MIT: Cambridge, 1989.

(27) Curtiss, L. A.; Raghavachari, K.; Pople, J. A. *J. Chem. Phys.* **1993**, *98*, 1293.

(28) Curtiss, L. A.; Raghavachari, K.; Trucks, G. W.; Pople, J. A. *J. Chem. Phys.* **1991**, *94*, 7221.

(29) Pople, J. A.; Head-Gordon, M.; Raghavachari, K. *J. Chem. Phys.* **1987**, *87*, 5968.

(30) *Handbook of Chemistry and Physics*, 74th ed.; Lide, D. R., Ed.; CRC: Cleveland, OH, 1993.

(31) This expression may be obtained via appropriate generalizations (as in ref 32) of the results provided in, e.g., Chesnavich, W. J.; Bowers, M. T. *J. Phys. Chem.* **1979**, *83*, 900.

(32) Wang, H.; Hase, W. L. *J. Am. Chem. Soc.* **1997**, *119*, 3093.

(33) Klippenstein, S. J. *J. Phys. Chem.* **1994**, *98*, 11459.

(34) Turulski, J.; Niedzielski, J. *J. Chem. Soc., Faraday Trans. 2*, **1988**, *84*, 347; *Mol. Phys.* **1989**, *67*, 181; *J. Chem. Phys.* **1989**, *91*, 3795; *Chem. Phys.* **1990**, *146*, 273; *Int. J. Mass Spectrom. Ion Processes* **1991**, *108*, 23. Turulski, J.; Niedzielski, J.; Pezler, B. *Chem. Phys.* **1992**, *166*, 115. Turulski, J.; Niedzielski, J.; Sakimoto, K. *Chem. Phys.* **1993**, *174*, 387.

(35) Smith, S. C.; Troe, J. *J. Chem. Phys.* **1992**, *97*, 5451.

(36) Dateo, C. E.; Clary, D. C. *J. Chem. Phys.* **1989**, *90*, 7216. Clary, D. C.; Dateo, C. E.; Smith, D. *Chem. Phys. Lett.* **1990**, *167*, 1.

(37) Smith, S. C. *J. Chem. Phys.* **1991**, *95*, 3404.

(38) Klippenstein, S. J. Unpublished results.